Fabrication and characterisation of poly(sulfonated) and poly(sulfonic acid) dissolving microneedles for delivery of antibiotic and antifungal agents

International Journal of Pharmaceutics 644 (2023) 123292

Contents lists available at ScienceDirect

International Journal of Pharmaceutics

journal homepage: www.elsevier.com/locate/ijpharm

Fabrication and characterisation of poly(sulfonated) and poly(sulfonic acid) dissolving microneedles for delivery of antibiotic and antifungal agents

Akmal Hidayat Bin Sabri [a,1], Qonita Kurnia Anjani [a,1], Pratik Gurnani [b], Juan Domínguez-Robles [a], Natalia Moreno-Castellanos [c], Li Zhao [a], Aaron R.J. Hutton [a], Ryan F. Donnelly [a,*]

[a] School of Pharmacy, Queen's University Belfast, Medical Biology Centre, 97 Lisburn Road, Belfast BT9 7BL, UK
[b] Division of Molecular Therapeutics and Formulation, School of Pharmacy, University of Nottingham, Nottingham NG7 2RD, UK
[c] Basic Science Department, Universidad Industrial de Santander, Bucaramanga 680001, Colombia

ARTICLE INFO

Keywords:
Poly(2-acrylamido-2-methyl-1-propanesulfonic acid)
Itraconazole
Levofloxacin
Microarray patches
Skin and soft tissue infections

ABSTRACT

Skin and soft tissue infections (SSTIs) arise from microbial ingress into the skin. In this study, poly(2-acrylamido-2-methyl-1-propanesulfonic acid) (polyAMPS), which has been reported to exhibit antimicrobial properties was synthesised for the manufacture of microarray patches (MAPs). The free acid and sodium salt of polyAMPS with controlled molar masses and narrow dispersity were synthesised *via* reversible addition − fragmentation chain-transfer (RAFT) polymerisation reaction with a monomer conversion of over 99%, as determined by ^{1}H NMR. The polymers were shown to be biocompatible when evaluated using a fibroblast dermal cell line while agar plating assay using cultures of *C. albican* demonstrated that the acid form of polyAMPS exhibited antimicrobial inhibition, which is potentiated in the presence of antimicrobial agents. The synthesised polymers were then used to fabricate dissolving MAPs, which were loaded with either ITRA or levofloxacin (LEV). The MAPs displayed acceptable mechanical resistance and punctured *ex vivo* skin to a depth of 600 μm. Skin deposition studies revealed that the MAPs were able to administer up to ~ 1.9 mg of LEV (delivery efficiency: 94.7%) and ~ 0.2 mg of ITRA (delivery efficiency: 45.9%), respectively. Collectively, the synthesis and development of this novel pharmaceutical system may offer a strategy to manage SSTIs.

1. Introduction

Skin and soft tissue infections (SSTIs) is an umbrella term that covers a range of infections of varying presentation, complex aetiology and a severity that arises from microbial invasion into the viable layers of the skin (Edelsberg, 2009; Hua, 2023). The aetiology of skin and soft tissue infections can be complex, due to the diverse microbiome present within skin tissues. In some instances, changes to the skin microbiome, termed dysbiosis, may induce SSTI (Gimblet, 2017; Dong, 2022). Some of the most common organisms that cause skin and soft tissue infections are *Enterococcus species, Pseudomonas aeruginosa, Staphylococcus aureus, Escherichia coli* and *beta-hemolytic Streptococcus* (Rajan, 2012).

Ideally, the treatment choice for SSTI is tailored to the causative microorganism. That said, in most cases, broad-spectrum antibiotics are administered first before microbiological results become available. Gentamicin and levofloxacin (LEV) are examples of broad-spectrum antibiotics that are administered to treat skin infections (Lawrence and Nopper, 2012). However, the aqueous solubility of these drugs limits their permeation across the highly lipophilic *stratum corneum* which render the drugs unsuitable to manage deep rooted SSTI (McAlister, 2020; McAlister et al., 2021). In addition, it is common for most antimicrobial agents that are used in the management of SSTI to display physiochemical properties that limit their permeation into the skin. Considering this limitation, microarray patches (MAPs) may help augment the delivery of antibiotics into the deeper strata of the skin (Sabri, 2019; Anjani, 2023).

* Corresponding author at: Chair in Pharmaceutical Technology, School of Pharmacy, Queen's University Belfast, Medical Biology Centre, 97 Lisburn Road, Belfast BT9 7BL, Northern Ireland, UK.
E-mail address: r.donnelly@qub.ac.uk (R.F. Donnelly).
[1] Joint First Authors: Akmal H Sabri and Qonita Kurnia Anjani.

https://doi.org/10.1016/j.ijpharm.2023.123292
Received 26 May 2023; Received in revised form 31 July 2023; Accepted 1 August 2023
Available online 6 August 2023

The emergence of antibiotic resistance mechanisms, coupled with the restricted selection of antibiotics available, reduces the number of efficacious treatments to manage SSTIs (Sabri et al., 2022; Kirkby et al., 2021). Therefore, it is of great importance to explore alternative strategies that could augment the action of already existing antimicrobial agents. During recent decades, several strategies have been explored in an attempt to delay the development and spread of antibiotic resistance. These strategies include the use of anti-virulence agents that interfere with bacterial quorum sensing, the utilisation of combinatorial therapy, which entails the use of multiple antibiotics concomitantly during treatment (Eliopoulos and Eliopoulos, 1988), as well as administering a mixture of antibiotics in tandem with adjuvants (Douafer et al., 2019). The later approach involves the co-administration of the antibiotic with a separate compound which does not typically exhibit antimicrobial properties, but may exert an inhibitory action on bacterial growth, or even augment the delivery efficiency of the drug, in order to obtain a synergistic antimicrobial effect. This approach aims to preserve the efficacy of currently available antibiotics and enhance their efficacy. In these instances, these compounds are known as "adjuvants." Alternatively, these compounds are also known as "resistance circuit breakers," "chemosensitisers," or "antibiotic potentiators" (Melander and Melander, 2017).

During the early period of antimicrobial MAP research, coated MAPs were the most utilised class of MAPs to administer potent antimicrobial agents for localised SSTIs (Gittard, 2013; Boehm, 2015; Sachan, 2017). However, this class of MAPs faces the challenge of limited drug loading, which may result in the delivery of sub-inhibitory concentrations of the antimicrobial agents into the skin. Therefore, it should come as no surprise that some researchers reported that this type of MAPs was ineffective in mitigating the growth of some strains of pathogenic microorganisms (Boehm, 2015; Boehm, 2016; Gittard, 2011). Additionally, the delivery of sub-inhibitory concentrations of antimicrobial agents to the infected skin site may not only cause treatment failure, but the sub-inhibitory concentrations delivered may exert a selective evolutionary pressure on the remaining microbes that could lead to development of antimicrobial resistant pathogens. Selective evolutionary pressure in this instant refers to a condition that causes a particular organism, in this instance pathogenic bacteria, to evolve in a certain direction which is advantageous to the survival of the pathogen. It is not a physical force but refers to a complex interplay between natural biological variation within a bacterial species and factors in its environment (e.g. antibiotic concentration) that cause a certain form to have an advantage over the others. In this example, there would be some population of pathogenic bacteria within the skin which harbour genetic advantages that confer some level of resistance to sub-inhibitory concentration of antimicrobial agents. When placed in a condition where sub-inhibitory concentration of antimicrobial agents is present, these population of bacteria will survive and grow resulting in an increase in the number of bacteria antibiotic resistant organism within the bacteria population. This is further coupled by the natural occurrence of antigenic drift within bacterial populations that would ultimately give rise to a group of bacteria that would have high resistance to a particular antibiotic (Palmer et al., 2016).To circumvent this, researchers have explored other variants of MAPs, particularly dissolving and hydrogel-forming MAPs for the treatment of SSTIs (Sabri et al., 2022; Permana, 2020; Peng, 2021).

To date, most studies have focussed on changing and modifying the payload within MAPs, whilst still employing commercially available pharmaceutical polymers. Another strategy that could be adopted to circumvent the rise of antimicrobial resistance is the co-administration of antimicrobial drugs with an antibiotic potentiator, which also serves as a polymeric excipient in the fabrication of MAPs. In the current study, we detail for the first time, the synthesis and preparation of MAPs from poly(2-acrylamido-2-methyl-1-propanesulfonic acid) (polyAMPS), a sulfonated polymer which has been reported to display antimicrobial properties. The use of polyAMPS as a potential antimicrobial potentiator in developing antimicrobial loaded dissolving MAPs is based on the work of Peddinti *et al.* (Peddinti, 2019); who demonstrated that the presence of a sulfonated group within charged multi- block polymers conferred self- sterilizing activity against a wide range of Gram-positive and -negative bacteria (Donnelly, 2009). More recently Farag *et al.* also showed that polyAMPS exhibit inhibition effects against Gram-positive and Gram-negative bacteria as well as fungal strains (Farag, 2020) while Botwina *et al.* (Botwina, 2022) have also shown that the use of polyAMPS and its co-polymer in fabricating self-organised nanoparticles also displayed anti-viral properties against Zika virus. In addition, we have opted to synthesise polyAMPS *via* reversible addition-fragmentation chain-transfer (RAFT) polymerisation as this approach generates polymer with narrow dispersity and excellent control of molecular mass and architecture (Fairbanks et al., 2015). In addition, as RAFT is considered as a form of living or controlled radical polymerisation, any polymer generated by this approach will still be suitable for subsequent copolymerisation and modification (Moad and Polymerization., 2012; Veloz Martínez et al., 2022). Besides that, through judicious choice of monomers and initiators, researchers may even opt to conduct RAFT polymerisation in water, without the use of any organic solvent, which emulates the principle of green chemistry (Gurnani, 2020). Overall, the use of this antimicrobial polymer may be of great benefit for the delivery of antimicrobial compounds used to treat SSTI, as these polymers may help improve the efficacy of the payload being delivered. This has the potential to provide an alternative drug delivery strategy for intradermal administration of antibiotics and antifungal agents into the skin.

2. Materials and methods

2.1. Materials

Levofloxacin hemihydrate (purity, 98%) (LEV) was sourced from Alfa Aesar (Lancashire, UK). Itraconazole (ITRA) (purity, 98%) was procured from Tokyo Chemical Industry (Oxford, UK). 2-Acrylamido-2-methyl-1-propanesulfonic acid (AMPs) was purchased from Sigma-Aldrich (Darmstadt, Germany). Poly(vinylpyrrolidone) (PVP) 90 kDa was kindly donated by Ashland (Kidderminster, UK). HPLC grade water was supplied using a water purification system (Elga PURELAB DV 25, Veolia Water Systems, Dublin, Ireland). Remaining chemicals and materials used in the work were sourced from Sigma-Aldrich (Dorset, UK) or Fisher Scientific (Loughborough, UK), all these reagents were of analytical grade. Full thickness skin used for this work was obtained from stillborn piglets within 24 h *post-mortem* and frozen at − 20 °C prior to any experiment.

2.2. Synthesis of poly(2-acrylamido-2-methyl-1-propanesulfonate), polyAMPS via reversible addition − fragmentation chain-transfer polymerisation

Poly(2-acrylamido-2-methyl-1-propanesulfonic acid) (polyAMPS) (sodium salt) was synthesised through aqueous reversible addition-fragmentation chain-transfer (RAFT) polymerisation. AMPs(1 g, 4.8 mmol) was dissolved in deionised water (3.2 mL) containing an equivalent amount of NaOH (0.192 g, 4.8 mmol) in a 4 mL vial. Chain transfer agent propanoic acid butyl trithiocarbonate (PABTC, 4.1 mg, 17.2 μmol) and initiator VA-057, 2,2′-Azobis[N-(2-carboxyethyl)-2-methylpropionamidine]tetrahydrate (0.35 mg as 17.8 μL of 20 mg/mL aqueous stock solution, 0.862 μmol) were introduced to the vial. The vial was charged with an appropriate 10 mm Teflon coated stir bar and sealed with an appropriate sub-seal. The polymerisation mixture was then purged of oxygen by bubbling with dinitrogen and immersed in a pre-heated oil bath at 70 °C for 3 h. The polymerisation mixture was then dialysed (Spectra-Por4 dialysis tubing, cut-off 3,500 Da MWCO, Spectrum Laboratories Inc., New Brunswick, NJ, USA) against deionised water for 36 h with 2 changes of dialysis water and subsequently lyophilised. The

isolated yellow powder was analysed by ^{1}H NMR spectroscopy and size exclusion chromatography to confirm purity and molar mass. PolyAMPS (acid) was synthesised with the same conditions without addition of NaOH for deprotonation.

2.3. Characterisation of polyAMPS

2.3.1. ^{1}H NMR

^{1}H and ^{13}C NMR spectra were recorded on a Bruker DPX-400 spectrometer using deuterated solvent. Measurements were performed at 25 °C using standard conditions (16 scans).

2.3.2. GPC

SEC analysis was performed using an Agilent 1260 instrument (Agilent UK Ltd, Stockport, UK) fitted with a differential refractive index detector. The system was equipped with 2 × Aquagel columns (300 × 7.5 mm) and an Aquagel 5 μm guard column. The eluent used was an aqueous solution of $NaNO_3$ (0.1 M). The polymers were eluted at 1 mL/min and prepared at 2 mg/mL. A calibration plot between 162—6,035,000 g/mol were prepared using PEG standards (Agilent EasyVials). Cirrus GPC software was utilised to analyse the GPC data in order to ascertain experimental molar mass ($M_{n,SEC}$) and dispersity (Đ) for the polyAMPS synthesised.

2.4. Preparation of itraconazole-polyAMPS powder blend

Polymeric solutions of either the salt or acid form of polyAMPS (1% w/v) were prepared in deionised water. Initially, 400 mg of ITRA and 6 mL of polyAMPS solution along with magnetic bars (8 × 4 mm, $n = 4$) and 8000 mg of ceramic beads, displaying particle size of 100 μm were mixed into the same borosilicate vial. This was then vortexed for 0.5 mins at a rate of 2500 rpm. Subsequently, the vial was secured to an IKA RCT Basic Magnetic Stirrer (IKA, Staufen, Germany), and agitated at 1500 rpm overnight. After that, the slurry was passed through a 200 mesh sieve and the collected mixture was stored at −80 °C for 3 h. The frozen drug-polymer mixture was lyophilised (VirtisTM Advantage XL-70, SP Scientific, Warminster, PA, USA) overnight following a cycle of − 40 °C for primary drying and 25 °C for secondary drying with a pressure of 50 m Torr.

2.5. Preparation of levofloxacin-polyAMPS powder blend

The powder blend of LEV was prepared by mixing 400 mg of LEV and 6 mL of the same polymeric solution outlined in Section 2.4, using the SpeedMixer™ (GermanEngineering, Hauschild & Co. KG, Hamm, Germany) for 180 secs at a rate of 3500 rpm. Following this, the mixture was frozen at −80 °C for 180 mins before being lyophilised overnight.

2.6. Fabrication of dissolving MAPs

Drug loaded MAPs were prepared based on our previous work (Peng, 2021). In short, a powdered blend of ITRA and solid dispersion of LEV were individually mixed with deionized water with a ratio of 1:3 (drug loaded powder: deionized water) using a SpeedMixer™ at 3,500 rpm for 5 mins. The first layer was cast by pouring 50 mg drug-polymer mixture into silicone moulds (16 × 16 pyramidal needle density, 850 μm height, 300 μm width at base, 300 μm interspacing and 0.36 cm^2 patch area) Fig. 1. A positive pressure of 4 bar was exerted onto the PDMS mould for 300 s. Any remaining mixture was meticulously scrapped off before the PDMS moulds were centrifuged for 10 min at 5,000 rpm. The MAPs were left at room temperature for 6 h before a backing layer, 0.85 mL, consisting of 30% w/w of PVP (90 kDa) and 1.5% w/w of glycerol was pipetted above the needle layer. The system was centrifuged for 10 mins at before being dried at room temperature for 24 h. Once dried, the MAPs were carefully removed and placed in a thermostatically controlled oven at 37 °C for 24 h. This was done to remove any remaining moisture present within the MAP.

2.7. MAP height reduction and ex vivo skin insertion study

The structure of the polyAMPS-based MAPs was visualized using a stereo microscope (Leica EZ4 D, Leica Microsystems, Milton Keynes, UK) and a scanning electron microscope (SEM) (Tabletop Microscope TM3030, Hitachi, Krefeld, Germany). The MAPs height reduction due to compression were evaluated using a TA-TX2 Texture Analyser (TA) (Stable Microsystems, Haslemere, UK). This was done by placing the MAPs under a compressive force of 32 N, the overall height reduction of the needles was calculated using Equation (1).

$$Height\ reduction\ (\%) = \frac{H_{before} - H_{after}}{H_{before}} \times 100\% \quad (1)$$

The ability of the manufactured MAPs to puncture both the skin simulant, Parafilm® M and *ex vivo* neonatal porcine skin was investigated *via* EX-101 optical coherence tomography (OCT) (Michelson Diagnostics Ltd., Kent, UK).

2.8. Drug loading localised in the needles

The MAP was dissolved in 5 mL of deionised water and agitated for 0.5 h *via* sonication. After the baseplates were totally dissolved, a 5 mL aliquot of methanol or acetonitrile was added to the mixture containing LEV and ITRA, respectively. The mixture was vortexed at 2,500 rpm for 1 min, then placed in a sonicator for 30 min. Finally, all samples were diluted, if necessary, and filtered, prior to HPLC injection for the quantification.

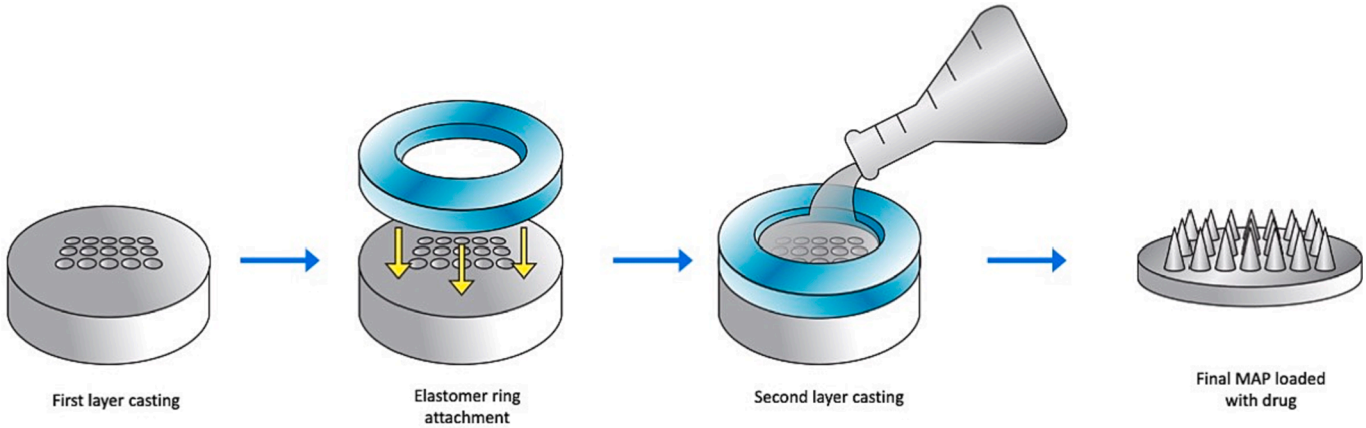

Fig. 1. Flow diagram showing the manufacturing process for polyAMPS-based MAPs.

2.9. In vitro skin deposition study

The deposition of ITRA and LEV into the skin from polyAMPS-based MAPs was investigated using a vertical Franz cell set up (Permergear, Hellertown, PA, USA). Using excised full-thickness neonatal porcine skin, the cell was assembled by attaching the skin to the donor chamber. The receptor chamber was filled with PBS (pH 7.4) which was degassed and pre-warmed to 37 °C. The polyAMPS-based MAP was inserted into the porcine skin *via* manual thumb pressure for 30 secs before the donor and receptor chamber were assembled and secured using a metal clamp. A stainless-steel cylinder weighing 5.0 g was placed above the MAPs to reduce the likelihood of the patch being dislodged from the skin during the permeation study. The permeation set up was maintained at 37 ± 1 °C under a constant stirring of 600 rpm. After 24 h, the experimental set up was disassembled. The skin along with the receptor fluid was collected for sample analysis. Drug extraction from the skin was performed by first homogenizing the skin with 500 μL of HPLC grade water using a Tissue Lyser™ (Qiagen, Ltd., Manchester, UK) for 15 mins. The samples were treated with either 1 mL of methanol (for LEV samples) or 1 mL of acetonitrile (ITRA samples) before undergoing the same homogenization cycle. The skin samples were agitated for 60 mins *via* sonication before being passed through a 0.2 μm nylon membrane (Agilent Technologies, Agilent UK Ltd, Stockport, UK) prior to HPLC analysis. With respect to the receptor fluid, the solution was diluted with 8 mL of either methanol (for LEV) or acetonitrile (for ITRA) before being agitated for 60 mins under sonication. The receptor fluid was then centrifuged for 15 mins at a speed of 14500 rpm. The supernatant obtained was subsequently sampled for HPLC analysis.

2.10. Biocompatibility study

The biocompatibility of polyAMPS on fibroblast-3T3L1 cells was evaluated using a similar method as published previously (Anjani, 2022). Briefly, the cells were plated and incubated with either the polyAMPS (sodium salt) or polyAMPS (acid) using Dulbecco's modified eagle medium (DMEM) culture medium (Sigma-Aldrich, St. Louis, MS, USA) for 72 h at 37 °C with 5% CO_2. The MTT assay was performed as published in our previous work. Once assayed, the optical absorbance was quantified using Synergy H1 microplate reader (Agilent Technologies, St. Clara, CA, USA) at 570 nm. In addition, a non-treated cell plate was used as a positive control while cells treated with Triton X-100 (1%) were utilised as a negative control. In addition, cell viability was evaluated using LIVE/DEAD™ as previously reported. On top of that, the ability of fibroblast-3T3L1 to proliferate was also studied *via* DNA content assay as published in our previous work. All the assays were performed in triplicates ($n = 3$).

2.11. Antimicrobial study

MAPs fabricated from either the acid or salt form of the polyAMPS and loaded with ITRA or LEV were tested for their inhibitory effect on cultures of *Candida albicans* NCYC 610 and *Staphylococcus aureus* NCTC 10788, respectively. This *in vitro* microbiological assay was performed based on a method described before (Peng, 2021). In brief, *C. albicans* was incubated for 24 h in Sabouraud dextrose (SD) broth at 30 °C. On the other hand, *S. aureus* was incubated at 37 °C for 24 h using Mueller–Hinton (MH) broth. Post-incubation, 50 μL of the cultures were pipetted into 5 mL of soft SD agar or soft MH agar for *C. albicans* and *S. aureus*, respectively. The mixtures were agitated and added to SD or MH agar plates. Subsequently, drug-loaded MAPs were introduced into the agar and incubated at 30 °C (*C. albicans*) and 37 °C (*S. aureus*) overnight. The zone of inhibition resulting from the formulation was quantified in mm. Additionally, inoculated plates with *C. albicans* or *S. aureus* alone and containing blank MAPs were also evaluated as positive and negative controls, respectively.

2.12. High performance liquid chromatography analysis

HPLC analysis (Agilent technologies 1220 Infinity, Agilent UK Ltd, Stockport, UK) was used to evaluate the drug loading and deposition of the formulation in accordance with International Council on Harmonisation (ICH) 2005 guidelines. Analysis of LEV was carried out using Luna Omega C18 (100 Å pore size, 10 mm length × 3.0 mm internal diameter; 3 μm particle size, Phenomenex, Cheshire, UK) while ITRA quantification was done using a Spherisorb® ODS1 column (150 mm × 4.6 mm internal diameter, 5 μm particle size) (Waters, Ireland). The analysis was conducted at 25 °C with samples being injected and eluted at 1 mL/min. The mobile phase, injection volumes, detection wavelength for LEV and ITRA are described in Table 1. Upon analysis, the data were processed using Agilent ChemStation® Software B.02.01.

2.13. Statistical analysis

The experimental data was evaluated using GraphPad Prism® version 8.0 (GraphPad Software, San Diego, CA, USA), with the data being shown as means ± standard deviation (SD), unless stated otherwise. When data from two different groups were compare, an unpaired *t*-test was conducted. In contrast, differences between multiple cohorts ($n > 2$) were evaluated using one-way analysis of variance (ANOVA). In both statistical tests, significance was deemed at p less than 0.05.

3. Results and discussion

3.1. Synthesis and characterisation of polyAMPS

In this study, derivatives of polyAMPS were synthesised, one being the sodium salt sulfonate derivative and the other a native sulfonic acid. The polymers were synthesised *via* RAFT polymerisation utilising the chain transfer agent PABTC under aqueous conditions. The ability to tailor RAFT polymerisation in accordance with the principles of green chemistry whilst permitting such rapid polymerisation highlight that RAFT holds great potential in synthesising polymers in an environmentally friendly manner for drug delivery (Semsarilar and Perrier, 2010). RAFT polymerisation involves reversible deactivation radical polymerisation, enabling polymerisation of vinylic monomers with controlled molar masses and narrow dispersity as shown in Fig. 2**.** This approach generated the polymeric excipient used in preparing the MAPs. In contrast, most pharmaceutical grade polymers that are used in fabricating MAPs, such as polyvinylpyrrolidone (PVP) and polyethylene glycol (PEG), are prepared by uncontrolled polymerisation reactions. This can result in wide dispersity, poor control of molecular mass and architecture of the polymer (Fairbanks et al., 2015) and unsuitability for subsequent copolymerisation (Moad and Polymerization., 2012). For both polymerisations, monomer conversions reached over 99% conversion, as determined by ^{1}H NMR spectroscopy. Aqueous SEC revealed both polymers had a narrow unimodal molecular weight distribution (polyAMPs (sodium salt) – $M_{n,SEC} = 36900$, $Đ = 1.27$; polyAMPs (acid) - $M_{n,SEC} = 39400$, $Đ = 1.22$), as expected for RAFT polymers. The narrow

Table 1
Parameters of HPLC analysis for LEV and ITRA quantification.

Analyte	Mobile phase	Injection volume	UV detection
Levofloxacin	0.02 M Potassium phosphate (with triethylamine 0.8%, pH 2.5 modified by addition of phosphoric acid): acetonitrile (85:15 v/v)	20 μL	295 nm
Itraconazole	Water (with triethylamine 0.05%, pH 8.0 modified by addition of phosphoric acid): acetonitrile (28:72 v/v)	20 μL	230 nm

(a) polyAMPS (sodium salt)

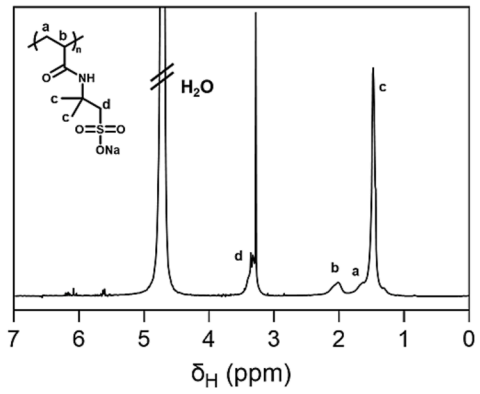

^{1}H NMR spectrum of polyAMPS sodium salt in D_2O measured at 25°C.

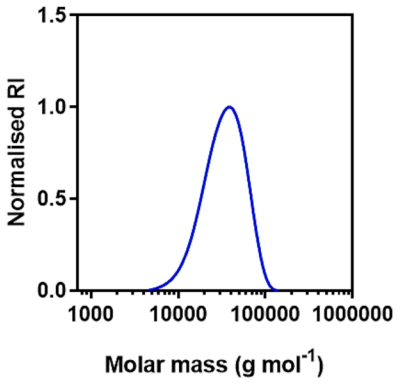

Aqueous SEC of polyAMPS sodium salt

(b) polyAMPS (sodium acid)

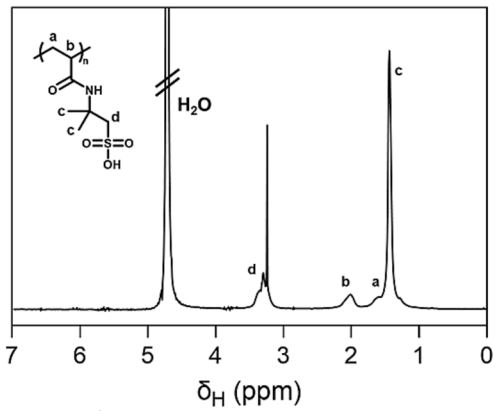

^{1}H NMR spectrum of pAMPS (acid) in D_2O measured at 25°C.

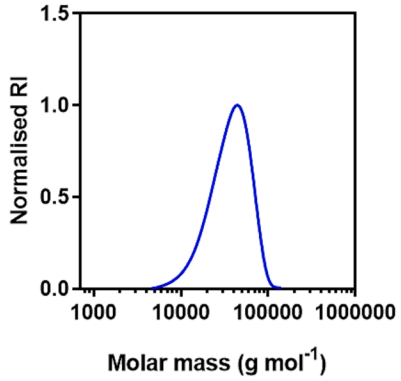

Aqueous SEC of polyAMPS (acid)

(c)

Polymer	Monomer conversion	$M_{n,SEC}$ (g mol^{-1})[a]	$M_{w,SEC}$ (g mol^{-1})[a]	$Đ^a$
pAMPS (salt)	>99%	36900	46700	1.27
pAMPS (acid)	>99%	39400	48200	1.22

Fig. 2. (a) ^{1}H NMR spectrum of polyAMPS (sodium salt) in D_2O measured at 25 °C and aqueous SEC of polyAMPS (sodium salt) (b) ^{1}H NMR spectrum of polyAMPS (acid) in D_2O measured at 25 °C and aqueous SEC of polyAMPS (acid). (c) Characterisation of the polymers synthesised in this study determined using Aqueous-SEC.

dispersity and control over polymer architectures, as evidenced by GPC and ^{1}H NMR may be of advantage in developing a polymer-based dissolving MAPs, as this would ensure that any polymer synthesised can be tailored to have a narrow molecular weight distribution below 60 kDa. This would ensure that the polymer deposited in the skin post MAP dissolution would be below the glomerular filtration threshold, enabling excretion *via* the kidneys once it reaches the systemic circulation (Hespe et al., 1977; Yamaoka et al., 1995).

3.2. Biocompatibility study

The biocompatibility of polyAMPS, both the salt and free acid forms, were assessed using a fibroblast like cell line. In this study, an MTT assay was used to determine any cytotoxic effects of the polymers. It can be seen from Fig. 3 that the result of the cell viability and proliferation assays in tandem with images from LIVE/DEAD™ staining is similar to the results previously reported by Anjani *et al.* (Anjani, 2022) which indicate that both the salt and the free acid forms of polyAMPS did not result in any reduction in cell viability. This indicates that the polymer itself does not induce any signs of toxicity within the cell line evaluated.

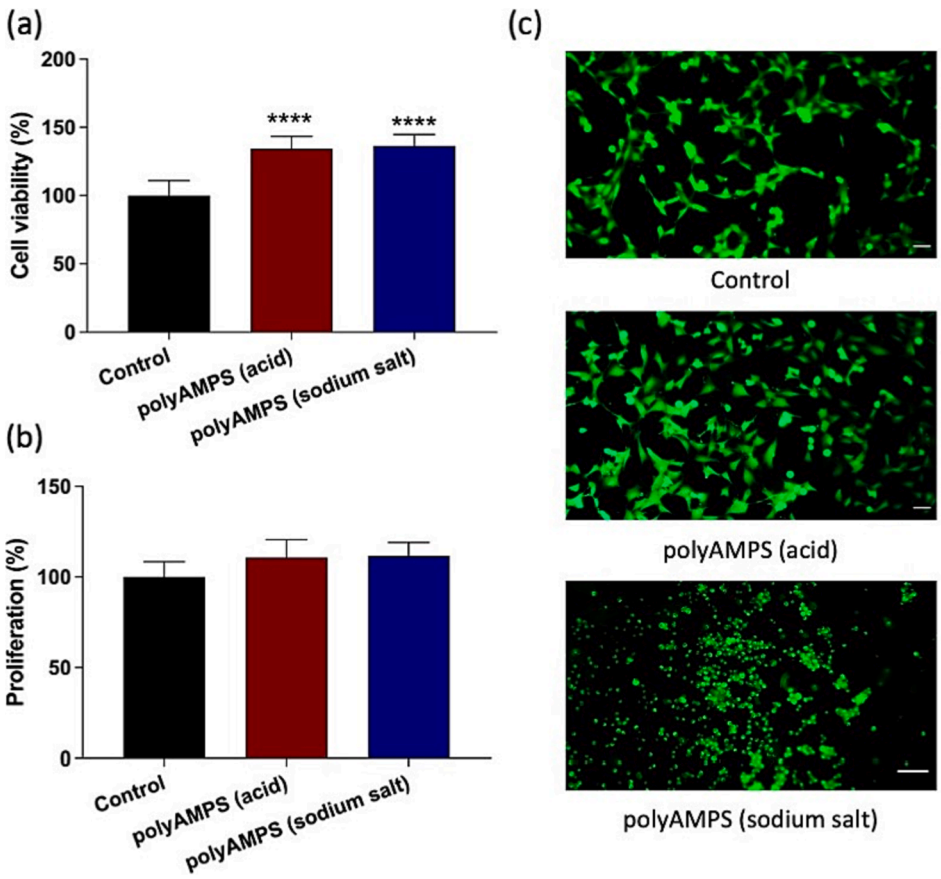

Fig. 3. (a) MTT assay results show viability of 3 T3 cells following treatment with either the salt or acid form of polyAMPS over a period of 3 days. (b) PicoGreen assay results showing proliferation of 3 T3 cells following treatment with either the salt or acid form of polyAMPS after 3 days. (c) Images of 3 T3 cells following Live/Dead™ staining (Green = FDA (live); red = PI (dead)); scale bar = 100 μm. Results are shown as means + SD (n = 6). (For interpretation of the references to colour in this figure legend, the reader is referred to the web version of this article.)

In addition, the results from the PicoGreen assay from Fig. 3 **(b)** showed that proliferation of 3 T3 cell line remained unaffected when the cells were treated with the salt and the free acid forms of polyAMPS. In addition, the absence of any red fluorescence from the Live/Dead™ staining in Fig. 3 **(c)** indicate the absence of extracellular nucleic acid. The release of nucleic acid is one of the principal signs of damaged plasma membranes arising from dead cells (Pasricha and Sachdev, 2017). Collectively, the observation from Fig. 3 **(c)** in tandem with the data shown in Fig. 3 **(a)** and Fig. 3 **(b)** support the finding that polyAMPS are indeed biocompatible with 3 T3 cell line. From a clinical standpoint, these observations suggest that the salt and the free acid forms of polyAMPS may be biocompatible and safe for skin administration.

3.3. Fabrication and characterisation of dissolving MAPs

3.3.1. Microscopy and solid-state analysis

Dissolving MAPs were fabricated from either the aqueous drug-polymer blend of polyAMPS and LEV, or from a powdered mixture of polyAMPS and ITRA, as depicted in Fig. 4 **(a)**. The resulting dissolving polymeric MAPs are shown in Fig. 4 **(b)** and **(c)**. It is apparent from the digital microscope and SEM images that all the MAPs consisted of sharp obelisk micro-projections on a flat and smooth base post micro-moulding. The blank MAPs and ITRA-loaded MAPs appeared transparent and clear as shown in Fig. 4 **(b)**. In contrast, LEV-loaded MAPs appeared slightly yellow, which may be attributed to the intrinsic colour of the antibiotic.

In addition, XRD analysis was conducted on the samples in order to evaluate the solid-state of LEV and ITRA powder that had been mixed with polyAMPS. It can be seen from Fig. 4 **(d)**, that both pure LEV and ITRA were present in a crystalline state prior to being formulated into dissolving MAPs. However, when mixed with polyAMPS, we noticed a reduction in the crystallinity of LEV, as evidenced by the reduction in the intensity of the XRD diffractogram. Additionally, the degree of crystallinity of LEV was similar when the drug was loaded with either the salt or free acid form of polyAMPS, which suggests that both forms of the polymer had a similar impact in reducing the crystallinity of LEV. With respect to ITRA, when the drug was mixed with the acid form of polyAMPS, we observed that the drug undergoes a reduction in crystallinity. This was evidenced from the reduction in peak intensity shown in the XRD diffractogram. This observation also suggests that some of the drug is still present in a crystalline state upon being mixed with polyAMPS. In contrast, when ITRA was formulated using the sodium salt form of polyAMPS, we observed that ITRA was present in an amorphous state as evidenced from the absence of any noticeable peaks in the XRD diffractogram.

One of the reasons why LEV may still be present in a crystalline state may be attributed to the process by which the solid dispersion of the drug was prepared prior to lyophilisation. With respect to LEV, the antibiotic was only mixed in the presence of polyAMPS for a brief period of 3 min which may not be sufficient in reducing the crystallinity of the drug. In the case of ITRA, a media milling approach was adopted in preparing the solid dispersion of the drug. This technique of preparing drug solid dispersion has been reported to not only reduce the particle size of the drug particles but in some instances may result in the amorphisation of certain drug molecules (Colombo et al., 2017). Nevertheless, it should be emphasised that the use of media milling in preparing drug solid dispersion does not necessarily result in the amorphisation of drug particles (Permana, 2020; Permana, 2019). This is also supported from the observation in the current work, which showed that ITRA was still present in a crystalline state when the antifungal drug was milled in the presence of the acid form of polyAMPS but undergoes amorphisation when milled with the salt of the polymer. Thus, it can be postulated that the process by which drug particles undergoes amorphisation in the presence of a polymeric excipient is indeed

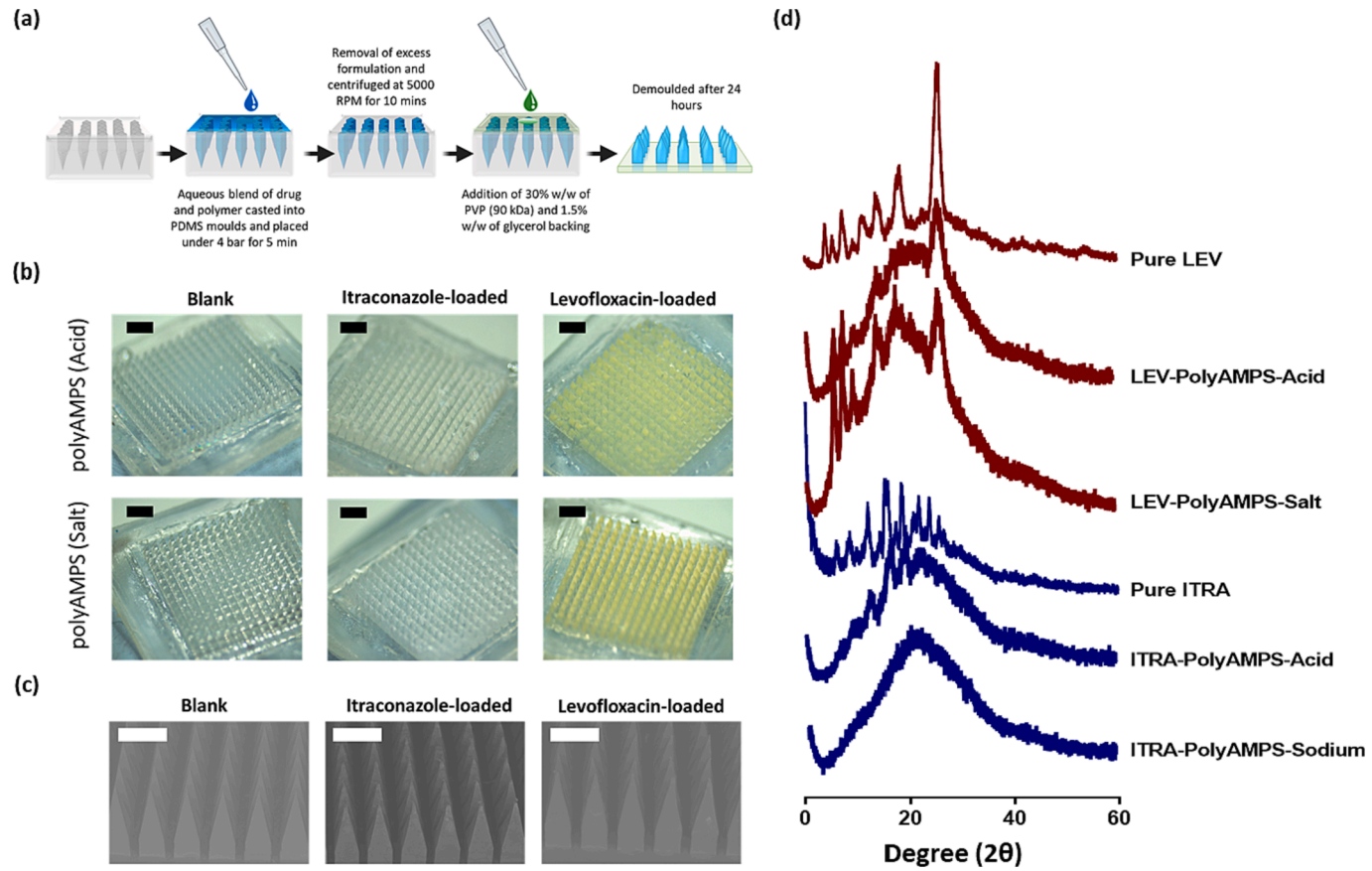

Fig. 4. (a) A schematic representation for the manufacturing procedures for polyAMPS based dissolving MAPs *via* double casting micromoulding. (b) Digital images of LEV and ITRA dissolving MAPs prepared from either polyAMPS (acid) or polyAMPS (sodium salt). In addition, a control formulation by which no drug was loaded into the needle layer were also fabricated from either polyAMPS (acid) or polyAMPS (sodium salt). Scale bar: 1000 μm. (c) SEM images of the MAPs to image the structure of microneedles. Scale bar: 500 μm. (d) Powder X-ray diffraction of pure drug (LEV or ITRA) and drug-polymer powder blend using either the acid or salt form of polyAMPS.

a multifactorial process, which is dependent on several parameters, such as surface energy, solubility, functional groups and even the viscosity of both the drug and the polymeric stabiliser (Peltonen and Hirvonen, 2010). However, in this work we have shown that, even when using the same polymer, in this instance polyAMPS, the form of the polymer (salt *vs* acid) impacted the final solid state of ITRA.

3.3.2. *Height reduction and insertion profile*

Following microscopic analysis of the MAPs, further characterisation studies were done to investigate the capability of the MAP formulations to be inserted into the skin. As displayed in Fig. 5 **(a)**, all the dissolving MAPs manufactured in this work exhibited a comparable reduction in height, 7–10%, when the needles experienced a compressive force of 32 N. It was apparent from Fig. 5 **(a)** that the utilisation of either acid or salt form of polyAMPS had no significant effect on the overall height reduction of the MAPs ($p > 0.05$) for the blank, ITRA and LEV loaded formulations. In addition, one-way ANOVA analysis of the formulation revealed no significant differences ($p > 0.05$) in height reduction for all the formulations investigated, despite the addition of the payload (ITRA and LEV) into the dissolving MAPs relative to blank MAPs (control formulation). In addition, the % height reduction observed in the current work were of similar values to other dissolving MAPs which were reported by other investigators (Permana, 2020; Tekko, 2022). Therefore, it is postulated that the MAPs manufactured in the current work displayed sufficient mechanical strength needed to breach the skin in order to deliver their payload for SSTIs.

It can be seen that we were able to load up to 0.5 mg of ITRA into polyAMPS-based dissolving MAPs. On the other hand, up to 2.0 mg of LEV was loaded into polyAMPS-based dissolving MAPS. As shown in Fig. 5 **(b),** using either the acid or salt form did not result in any significant difference ($p > 0.05$) in drug loading into the MAPs. The higher loading achieved with LEV relative to ITRA may be attributed to higher aqueous solubility of LEV (1.44 mg/mL) relative to ITRA (1.4 ng/mL) (Mellaerts, 2008). Upon evaluating the architecture, mechanical properties and drug content of polyAMPS-based dissolving MAPs, an insertion study into Parafilm® M was conducted in an attempt to elucidate the insertion profile of the MAPs fabricated. We used Parafilm®M as a skin simulant to evaluate needle insertion as this has been a standard test used in a majority of microneedle-based research (Sabri et al., 2022; Larrañeta, 2014; Volpe-Zanutto, 2022; Kurnia et al., 2022). Unlike the use of *ex vivo* skin, by inserting MAPs into Parafilm®M this provides us with the means of evaluating how the number of microneedle channels generated following patch application changes with insertion depth. The Parafilm®M insertion test can easily be implemented as a routine approach to evaluate formulations and to control the quality of the MAPs manufactured. This test can be viewed as a potential pharmacopeial, or quality test used to evaluate MAPs especially during scale-up production processes. The Parafilm®M test used in this study are typically used in complement with existing test for characterising MAPs. From Fig. 5 **(d-i)-(d-iii)**, all six MAP formulations exhibit comparable insertion profiles, with all the formulations breaching the first Parafilm® M layer, with an insertion efficiency of 100% as well penetrating the stack of Parafilm® M down to the fourth layer. Furthermore, we also observed that there were differences in the insertion profile between MAPs fabricated from either the salt or acid form polyAMPS, although these differences were more apparent in the latter Parafilm®M layers

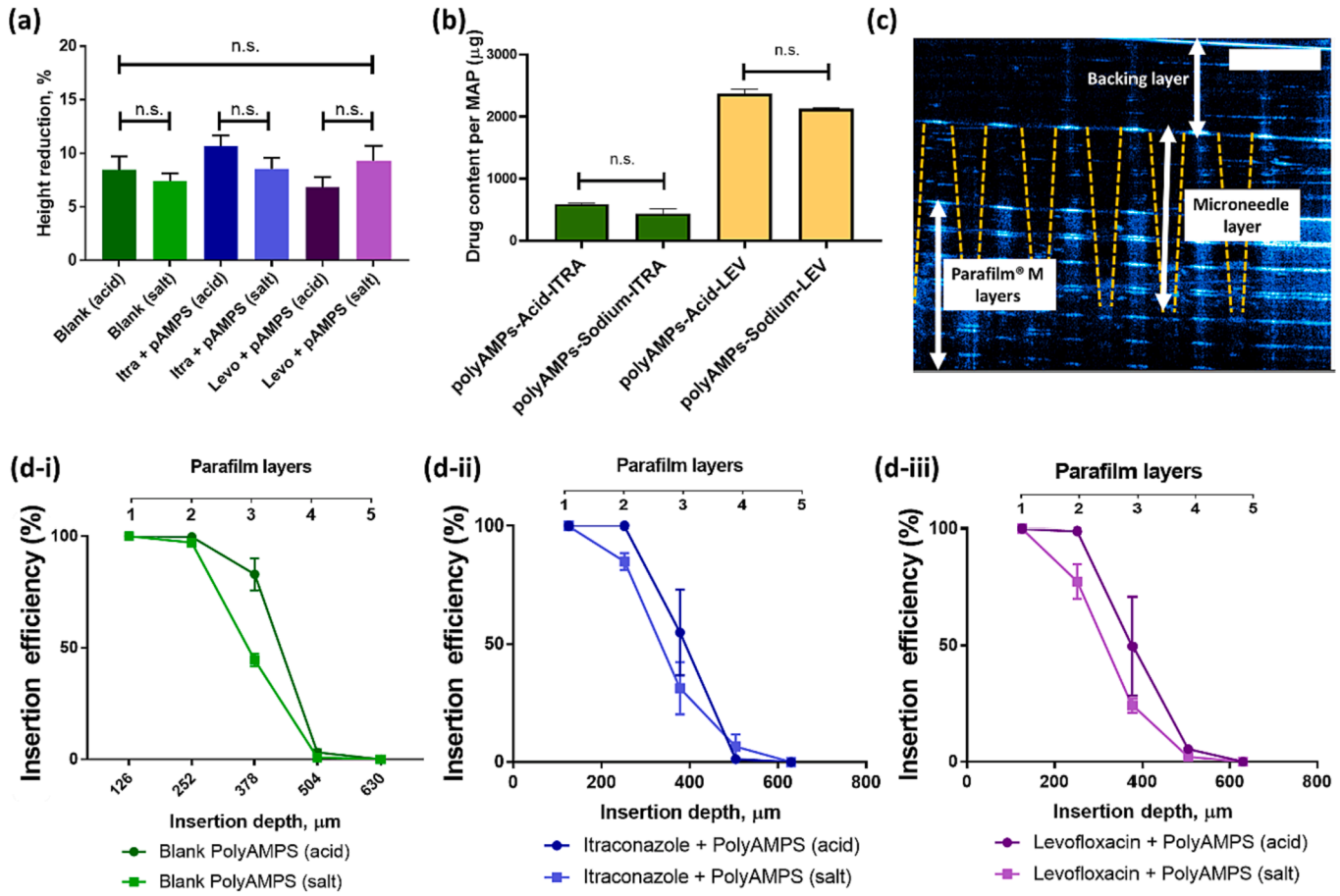

Fig. 5. (a) MAP height reduction for microneedles fabricated from polyAMPS without drug (blanks), loaded with the antifungal drug ITRA, loaded with the antibiotic LEV. The formulations were manufactured from either the acid or salt form of the polymer. The MAPs were compressed using 32 N (means + SD, $n = 20$). **(b)** ITRA and LEV content per MAP for both acid and salt forms of polyAMPS. (means + SD, $n = 3$). **(c)** Example of an OCT image depicting the insertion of polyAMPS-based dissolving MAPs into a stacked Parafilm®M layers. Scale bar: 500 μm. **(d)** Insertion efficiency, monitored *via* the % of holes across Parafilm® M layers for **(i)** blank PolyAMPS, **(ii)** ITRA and **(iii)** LEV loaded polyAMPS MAPs (means ± SD., $n = 3$).

(layer 2 and layer 3). One possible explanation for this observation is that when drug molecules, such as ITRA and LEV, are added into the needle layer of the polyAMPS MAPs, the free acid polymer is available to form hydrogen bond with the drug molecule which in turn result in a stronger MAP capable of achieving hinger insertion efficiency relative to the salt form of the polymer. It is postulated that this hydrogen bond is less likely to form with the salt form of the polymer as the R-S(=O)$_2$O$^-$ groups of the polymer is forming an ionic interaction with the Na^+ along the needle length. Nevertheless, in the absence of any drug molecules as shown in Fig. 5 **(d-i)**, this hydrogen bond interaction is less likely to occur resulting in similar insertion profile between the free acid and salt form of the polymer.

Subsequently, the penetration of the formulations was also evaluated using *ex vivo* neonatal porcine skin as shown in Fig. 6 **(a).** As depicted in Fig. 6 **(b)**, OCT was employed to monitor and visualise the *in situ* the depth the needles have been inserted into the skin. Based on Fig. 6 **(c)**, all six formulations penetrated the skin to a depth of ≈ 600 μm, despite having different payloads and being fabricated from different forms of polyAMPS. It was also observed from the OCT analysis that all MAP formulations that were fabricated from the acid form of the polyAMPS resulted in significantly ($p > 0.05$) deeper needle insertion relative to MAPs that were fabricated from the salt form of the polymer. Nevertheless, these differences did not impact the intended delivery site of the formulations, as the MAPs were successfully implanted into the epidermis and dermis. Indeed, the height of the MAP itself would have an impact on the drug payload delivered at the SSTI site. Although a longer MAP would enable a much deeper delivery and penetration of payload to the SSTI site, this longer MAP design would increase the risk of stimulating the dermal nociceptors and thus increasing the likelihood of pain during application. Initial work by Gill *et al.* have shown that microneedle should have a length of less than 960 μm in order to result in the lower pain sensation upon microneedle application (Gill et al., 2008). In addition, another study by Kirkby *et al.* have shown that a microneedle system ought to be able to deliver payload to a depth of approximately 400–700 μm into the skin as these are the region by which pathogen bacteria tend to reside during SSTI (Kirkby et al., 2021; Kirkby et al., 2022). Our recent work using MAP with a design of 850 μm length have shown that the system was capable of reaching a depth of ≈ 600 μm which is the target depth for the management of SSTI. In addition, as the length is much lower than 960 μm and this design poses a lower risk of causing pain upon application.

From a physiological standpoint, skin infections typically manifest from pathogenic bacteria that exist not only on the top layers of the skin, but also those that reside deep within the epidermis and dermis (Nakatsuji, 2013; Nakatsuji, 2013). Therefore, it is worth noting that loading the MAP formulations with either LEV or ITRA did not compromise the insertion profile of the formulation into the skin. Importantly, all four MAPs loaded with either ITRA or LEV were shown to penetrate to a depth of 600 μm. This indicates that ITRA and LEV MAPs have the required mechanical strength to deliver their payload into the dermal layers of the skin and target deep tissue pathogenic bacteria.

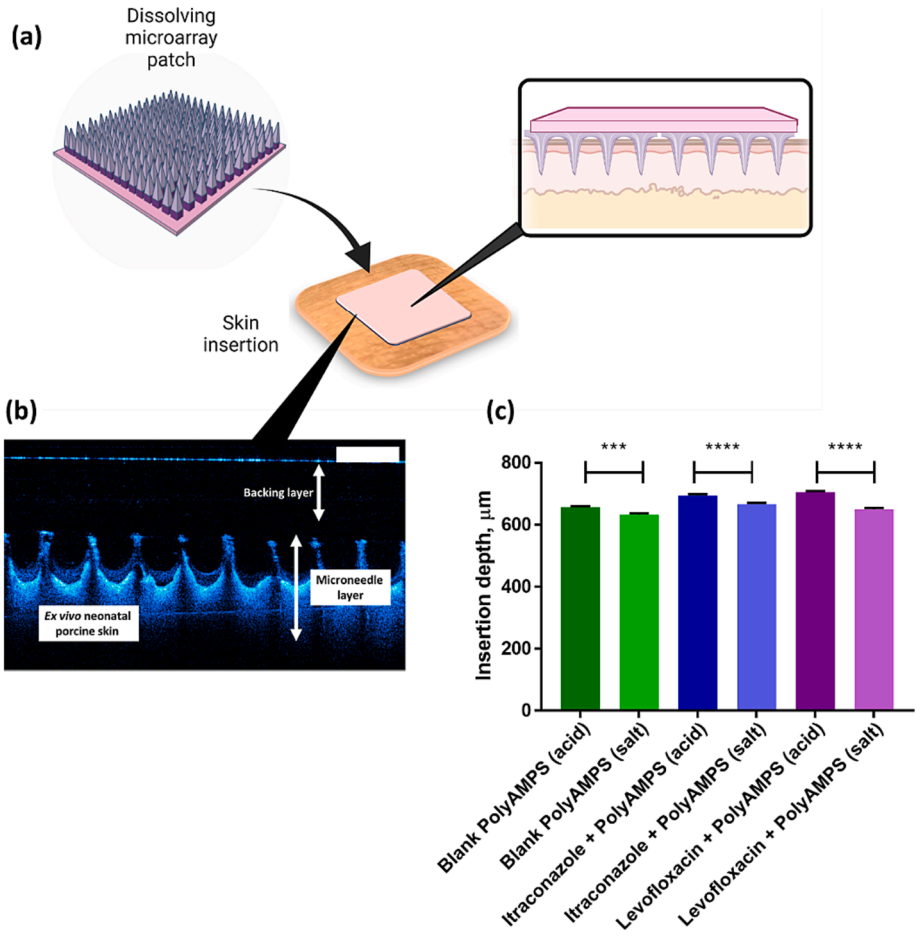

Fig. 6. **(a)** Schematic illustrating the insertion of a polyAMPS-based dissolving MAP into full thickness *ex vivo* porcine skin. **(b)** OCT image illustrating *in situ* MAP insertion into full thickness *ex vivo* porcine skin, scale bar: 1 mm. **(c)** Insertion depth of polyAMPS-based dissolving MAPs into *ex vivo* skin (means + SD., n = 20).

Upon conducting a series of insertion tests, we also studied the dissolution profile of the needles following MAP application to the skin. As shown in Fig. 7, we can see that after 1 h, we observed that a majority of the needle tip have dissolved following skin application for LEV loaded polyAMPS (sodium salt) and ITRA loaded polyAMPS (acid) based MAPs. In contrast, we noticed minimal needle dissolution with regards to LEV loaded polyAMPS (acid) and ITRA loaded polyAMPS (sodium salt) based MAPs. It could be postulated that the physiochemical properties of the drugs itself (ITRA *vs* LEVO) may affect the dissolution profile of both forms of polyAMPS (salt *vs* acid) causing the needles to exhibit similar dissolution profile within the skin. Nevertheless, after two hours of skin insertion we observed complete needle dissolution, tip, and shaft, for all four formulations investigated. This suggest the MAP formulation would require a total application time of 2 h in order to achieve significant if not complete delivery of the payload which is localised in the needle layer of the patch. The rapid dissolution profile for these patches may be attributed to the hydrophilic nature polyAMPS which is due to the presence of the highly charge sulfonate groups (Farag, 2020; Botwina, 2022).

3.4. *In vitro skin deposition study*

Following MAP characterisation, drug deposition from the MAP into and across the skin from the patches was investigated. It can be observed from Fig. 8 **(a)-(b)**, that LEV displayed a higher delivery efficiency and quantity of drug delivered relative to ITRA. This difference may be due to the higher aqueous solubility of LEV relative to ITRA. Furthermore, the higher aqueous solubility for LEV resulted in greater LEV permeation through the skin and into the receiver fluid, as displayed in Fig. 8 **(a)**. On the other hand, due to its low water solubility, ITRA was mainly deposited into the skin tissue, with minimal quantities being delivered into the receiver compartment, as shown in Fig. 8 **(b)**.

With respect to intradermal delivery of ITRA, formulators have explored the use of dissolving MAPs for the treatment of cutaneous candidiasis. For instance, Permana *et al.* (Permana, 2020) were the first to explore this strategy by employing the use of ITRA nanocrystals loaded into dissolving MAPs that were fabricated from the commonly used pharmaceutical polymers PVA and PVP. In their work, the researchers showed that this formulation strategy provided an effective means to enhance and localise the delivery of ITRA into the skin relative to a topical cream (Permana, 2020). Furthering this, Anjani *et al.* (Anjani et al., 2022) explored the influence of surfactants within PVA/PVP dissolving MAPs on the delivery of ITRA. In their work, they discovered that the addition of non-ionic surfactants, such as Pluronic® F88, Lutrol® F108 or Tween® 80, had no significant impact on the drug loading of the respective dissolving MAP formulations. However, when the formulations were administered into the skin, using a Franz cell setup, it was discovered that ITRA loaded into PVP/PVA MAPs in the presence of Lutrol® F108 achieved the highest delivery efficiency (37.44%) out of all the systems evaluated (Anjani et al., 2022). However, when this is compared to our current work, we observed that when ITRA was loaded into dissolving MAPs that were fabricated from the acid form of polyAMPS, an even higher delivery efficiency of 45.9% could be achieved. It could be postulated that this enhanced delivery

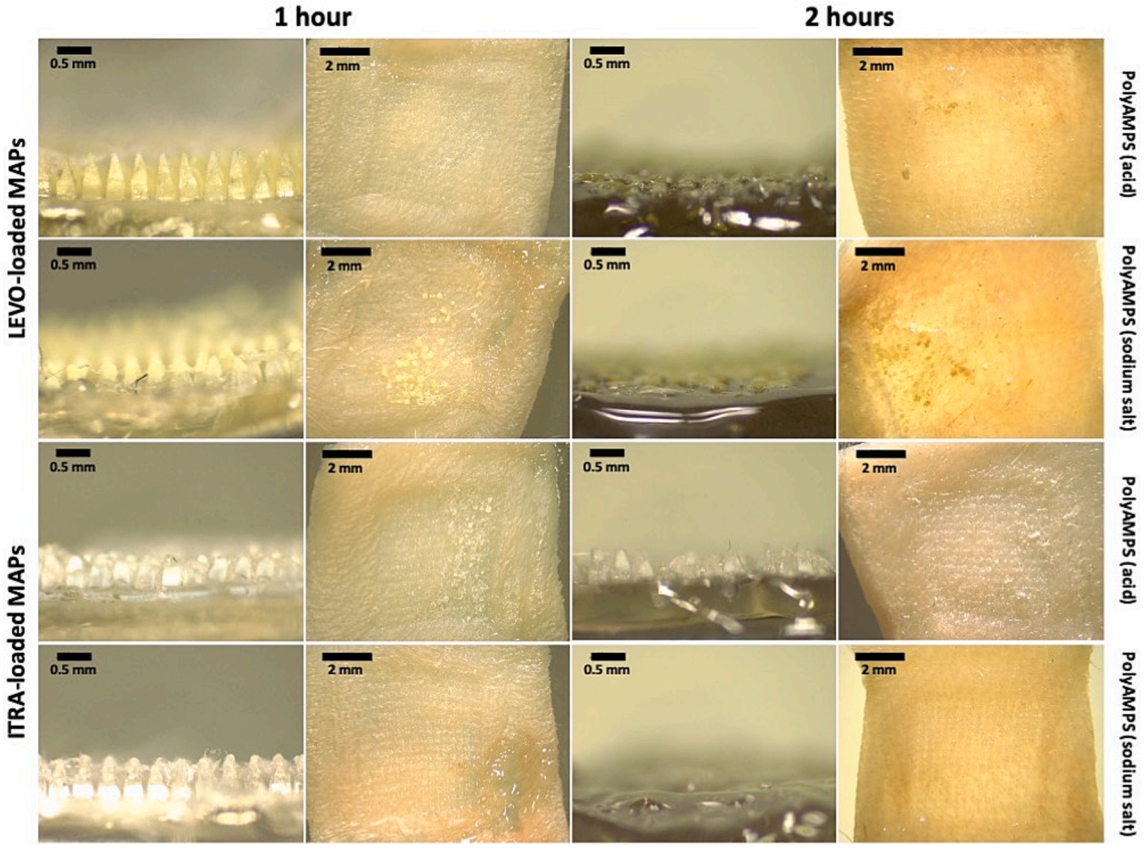

Fig. 7. Digital images of the dissolution of MAPs loaded with either LEV or ITRA using either the sodium salt or acid form of polyAMPS.

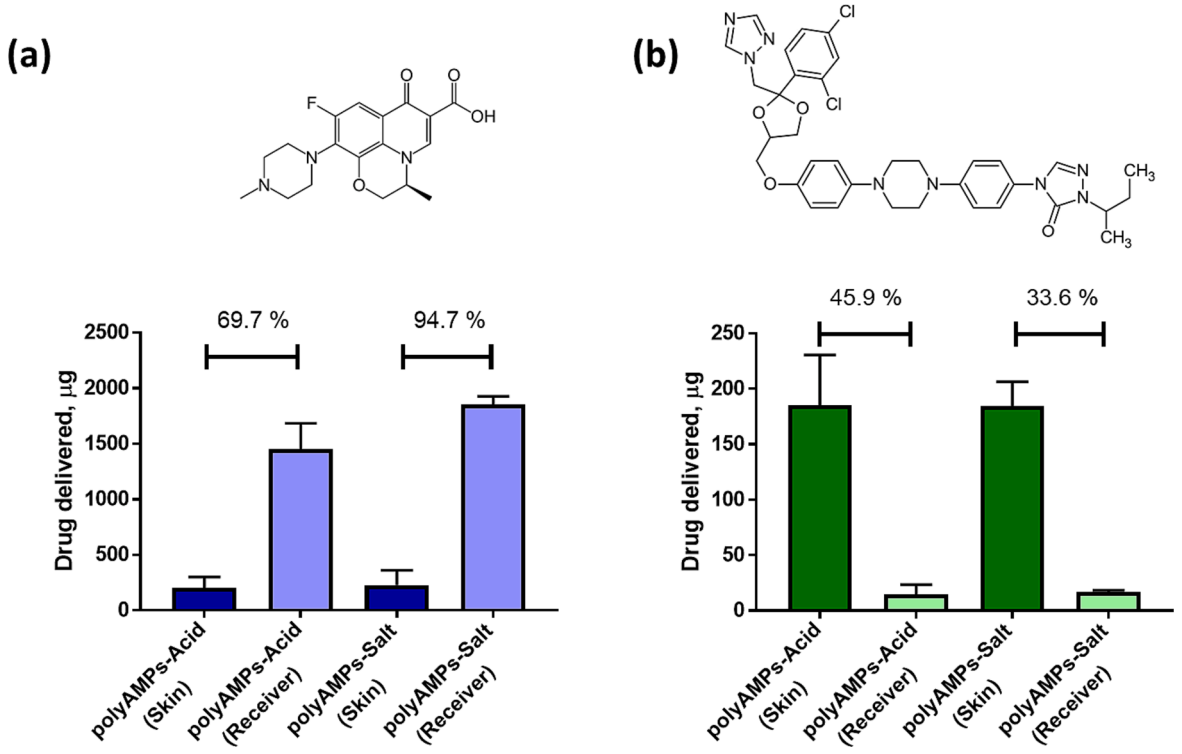

Fig. 8. In vitro skin deposition study of **(a)** levofloxacin (LEV) and **(b)** itraconazole (ITRA) from polyAMPS-based dissolving MAPs into and across full-thickness neonatal porcine skin following a Franz cell permeation study over the course of 24 h. Data are expressed as means + SD, n = 3. Percentages define the delivery efficiency of each drugs over 24 h.

efficiency may be attributed to the higher aqueous solubility of polyAMPS MAPs relative to PVP/PVA based MAPs Pubchem, 2022. Another plausible explanation may be attributed to the lower drug loading achieved with the current formulation, 500 μg, relative to the higher loading used by Anjani *et al.* (Anjani et al., 2022) which was ≈2000 μg. The lower drug loading may result in the MAP needle tips being less hydrophobic relative to a higher drug loading tip. This is evidenced from the water contact angle of the ITRA-polyAMPS films which were less than 50° as shown in **Table S1**. These values were much lower than the water contact angle values of the ITRA-polymeric films reported by Anjani *et al* 2022 which were 70°, thus indicating that the MAP needle tip prepared in the current work is much more hydrophilic (Anjani et al., 2022). This may result in greater needle dissolution upon application thus enhancing the delivery efficiency. It is worth noting that although the delivery efficiency achieved in the current work for ITRA-loaded dissolving MAPs are fairly similar to those reported for dissolving MAPs (Volpe-zanutto, 2021)(Zhang, 2023), the delivery efficiency achieved by these MAPs are far lower relative to LEV-loaded MAPs. Moving forward, one possible way to augment the delivery efficiency of polyAMPS based ITRA-loaded dissolving MAPs is to first reduce the particle size of ITRA into nanocrystals *via* media milling prior to loading the drug into polyAMPS-based dissolving MAPs. This is because prior work by Permana *et al.* have shown that this strategy provide an elegant approach to augment the delivery efficiency of dissolving MAPs (Permana, 2020). Additionally, the incorporation small quantities of surfactant, 1–5 % w/w into these dissolving MAPs, as shown by Anjani *et al.* may also be a possible approach to augment the delivery efficiency of polyAMPS based ITRA-loaded dissolving MAPs (Anjani et al., 2022).

As shown previously in Fig. 5 **(b)**, the use of the salt and acid form of the polymer during MAP manufacture did not have a statistically significant impact ($p > 0.05$) on the loading of LEV and ITRA into the dissolving MAPs. Based on the drug deposition study, it was apparent that the sodium salt and acid form of polyAMPS had an impact on the delivery efficiency of LEV and ITRA into the skin. With respect to LEV, it can be seen that using the sodium salt form of the polymer resulted in a greater delivery efficiency of LEV into and across the skin. In contrast, using the acid form of polyAMPS improved the delivery efficiency of ITRA, relative to the salt form of the drug. In our previous work with dissolving MAPs that were fabricated from PVA and PVP, we reported that incorporating surfactants, such as Pluronic®F88, Lutrol® F108 and Tween® 80 enhanced the delivery of the water-soluble drug, ibuprofen sodium by up to 78% (Anjani et al., 2022). However, in the present study, we observed that even the addition of polyAMPS (salt) enhanced the delivery efficiency of LEV, equivalent to 94.7%. Such high delivery efficiency achieved using polyAMPS may be attributed to the high aqueous solubility and superabsorbent properties of the polymer. These properties are due to the presence of several hydrophilic pendant groups, such as the sulfonic acid and amide group within the polyAMPS structure (Martínez-Cornejo, 2020). Although the MAPs in this work have been developed for the purpose of treating localised SSTIs, the difference in drug deposition observed here may provide future avenues that is worth exploring with regards to the target fungi and bacteria. For instance, the use of polyAMPS, both acid and salt, in combination with hydrophobic antimicrobial may be of great utility, as exemplified by ITRA loaded MAP, for the treatment of more localised fungal infection of the skin, such as the treatment of cutaneous candidiasis. In contrast, the use of the polymers in tandem with a more hydrophilic antimicrobial agents, as exemplified by LEV, may indicate that although the MAP has some value in treating localised bacterial infection, the system could also be further explored and refined for the treatment of systemic infection such septicaemia.

From a clinical standpoint, the ability of antibiotic and antifungal loaded MAPs to be applied directly to infected skin may be of therapeutic benefit to the patient. This is because SSTIs are conventionally managed *via* empirical antibiotic regimens which are administered orally, topically or by intravenous injection. These regimens, particularly in the case of LEV, are typically guided by plasma concentration of the antibiotic. Nevertheless, these administration routes may not be the most ideal strategy to deliver the antibiotic. For instance, studies have reported that these routes of administration may only result in sub-inhibitory concentrations of the drug being achieved in both soft tissues and deeper skin layers (Joukhadar, 2001). Furthermore, when the infection has taken place, inflammation may also ensue within these tissues. This can substantially affect tissue penetration of antimicrobial agents, due to compromised integrity of intradermal capillaries, oedema and altered composition of interstitial fluid within the affected tissue (AMPS, 2022). This has been shown to be especially true for antibiotics, such as β -lactams, fosfomycin, imipenem and moxifloxacin in patients with sepsis or those suffering from SSTI (Volpe-zanutto, 2021; PubChem, 2022). However, using the MAP approach, we have the potential to localise the delivery of these antimicrobial agents in a more targeted fashion to the affected tissue thus minimising any unwanted exposure of the antimicrobial agents to other parts of the body. This is especially true for the oral delivery of LEV, which could only achieve a skin tissue concentration of ≈11 μg/g following the administration of three oral, once-daily 750 mg doses of LEV (Zhang, 2023). Importantly, in this current study, we demonstrated that using a dissolving MAP strategy a localised tissue concentration of ≈314 μg/g could be achieved. This is far higher than the reported tissue concentration achieved *via* oral administration, thus highlighting the value of using dissolving MAPs as a more targeted formulation approach to managed localised SSTIs.

With regards to the practical application of these MAPs, we believe that the delivery of these antimicrobial agents directly to the site of infection relative to conventional therapy with oral antibiotic may offer a potential solution to obviate the likelihood of inducing gut dysbiosis. Currently, the delivery of LEV and ITRA for treating skin infections is commonly administered *via* oral formulation which can have devastating and potentially damaging effects on the gut microflora resulting in a reduction in taxonomic richness. Therefore, by delivering these antimicrobial agents *via* dissolving MAPs, which exhibit high delivery efficiency and rapid skin dissolution, we can achieve selective targeting of the payload to the infected skin site with minimal impact on the gut microbiome. Furthermore, with this targeted delivery approach, we are able to reduce the drug dose thus minimising the propensity of inducing toxicity following administration. With respect to skin application, the use of rapidly dissolving MAPs fabricated from polyAMPS, we can achieve complete drug deposition into the skin following a minimal wear time of 2 h. This is a clear advantage over conventional therapies such as cream and ointments which necessitates longer wear time, in addition to exhibiting poor skin permeation.

3.5. Antimicrobial study

The antimicrobial effect of the manufactured blank and drug loaded MAPs were tested on microorganism cultures of either *C. albicans* or *S. aureus*. The latter is probably the most commonly identified pathogen responsible for SSTIs (Martínez-Cornejo, 2020). Moreover, fungal infections in immunocompromised and critically ill patients are mainly caused by *Candida* spp. For instance, *C. albicans*, a normal constituent of the human microbiome, could breach deeper tissues when the cutaneous or mucous membrane barriers are temporarily compromised by disease, surgery, or trauma, thus causing SSTIs (Joukhadar, 2001). The results of the antimicrobial test, a disk diffusion test, are shown in the Fig. 9. MAPs made from either the acid or salt form of the polyAMPS that were loaded with ITRA or LEV exhibited a clear zone of inhibition in both *C. albicans* and *S. aureus* plates, respectively. Although the zones of inhibition were difficult to measure due to the MAPs composition (dissolving MAPs), the zones of inhibition in the *C. albicans* plates with ITRA-loaded MAPs were very similar, regardless of whether they were manufactured using either the acid or salt form of the polymer. Furthermore, the zones of inhibition in the *S. aureus* plates for both acid and salt forms of polyAMPS MAPs loaded with LEV were oval shaped with minor and major axes of *ca.*20 and 50 mm, respectively.

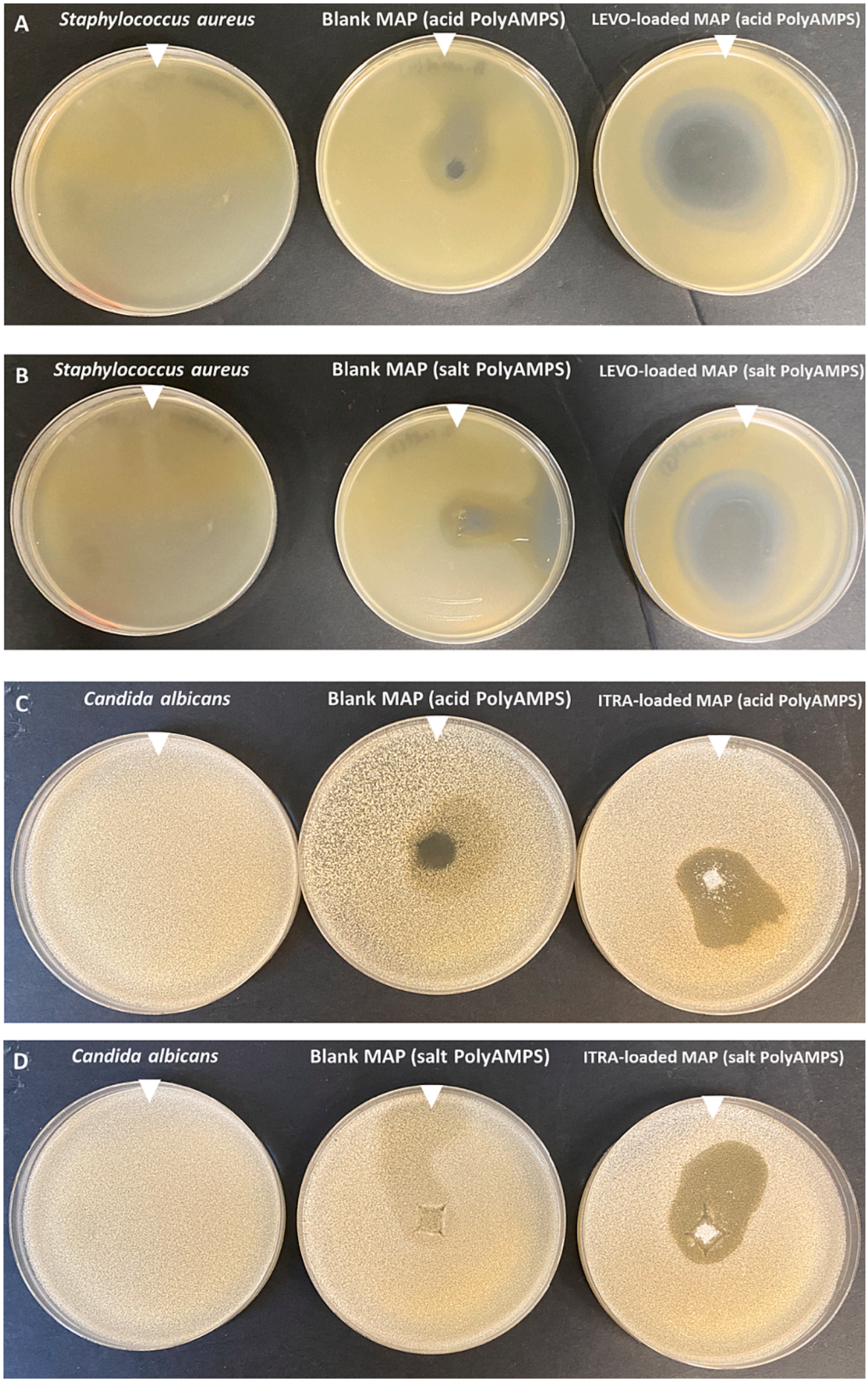

Fig. 9. A representative picture showing the zones of inhibition obtained for *S. aureus* (A-B) and *C. albicans* (C-D) in MH and SD agar plates, respectively.

MAPs containing no drug, fabricated from either the acid or salt form of the polyAMPS revealed limited signs of antimicrobial activity against *S. aureus*. The zones of inhibition were very small and difficult to distinguish in comparison to those caused by LEV-loaded MAPs. Moreover, both forms of polyAMPS were also tested against *C. albicans*. Although the salt form of the polymer did not inhibit fungal growth, the acid form displayed a small, but clear zone of inhibition (*ca.* 12.5 mm). Nevertheless, it is important to note that this zone of inhibition was considerably lower than the ones obtained with ITRA-loaded MAPs as shown in Fig. 9. Various dissolving MAP platforms loaded with different

drugs, such as ciprofloxacin (Bhatnagar et al., 2017) or amphotericin B (Peng, 2021) have also been used in *ex vivo* studies of *S. aureus* skin infections and cutaneous fungal infections, respectively. Moreover, different MAP platforms containing amphotericin B-loaded implantable tips have been used for the same purpose (Peng, 2021) . Accordingly, LEV- or ITRA-loaded MAPs may be a suitable and useful technology for the treatment of SSTIs which involve microbial invasion and ingress into the skin and underlying soft tissues.

Overall, this work showed that polyAMPS could serve as a potential excipient in the fabrication of dissolving MAPs for the delivery of antimicrobial agents. Nevertheless, considerable work is still needed in order to bring this formulation from the lab into the clinics. For example, drug delivery scientists, polymer chemists and engineers ought to work in tandem and closely with patients in order to detect any additional human factors that ought to be considered when fabricating the formulation for clinical application. For example, the thickness of the skin, especially the *stratum corneum* layer, displayed significant biological variability anatomically and even more between individuals. One potential solution that could be used in order to aid MAP application to the skin and provide some level of standardised and reproducible insertion is *via* the use applicators (Bhatnagar et al., 2017). In doing so, this would help eliminate the differences in force of application between individual at the application site and thus eliminate one confounding factor that contributes to the variability in MAP insertion depth. Additionally, future work within the field involving human factor studies ought to investigate the effect of different MAP designs (e.g., length, array size, patch area) on the needle insertion depth at different skin sites on the body using placebo needles. Such studies ought to have a robust study design that also evaluates the effect of age, gender, and race as this too would have a profound effect on needle insertion. Such human-based studies using placebo MAPs may help provide preliminary information needed in order to gauge if the MAP design is capable of reaching the target dermal depth needed in order to deliver the payload for SSTI. Should the insertion be subpar to the target depth, an alternative designs, or formulation approach would be warranted. Additionally, stability studies involving the use of relevant primary packaging for MAPs is also critical in order to identify the stability of the formulation upon storage and whether additional storage parameters are needed (McAlister et al., 2021). Presently, there is a disparity between the public awareness regarding the presence of MAP technology despite the progress and advancement within the field. Researchers ought to be actively engaging with end users *via* outreach events to help disseminate information regarding MAPs to the public. This would in turn generate a strong commercial demand for the technology.

4. Conclusion

Collectively, the present body of work demonstrates the synthesis, manufacture and assessment of polyAMPS based MAPs for the management of SSTI. The polymers were synthesised *via* RAFT polymerisation reaction, reaching a monomer conversion of over 99%. The resulting polyAMPS displayed a unimodal M_w distribution, narrow dispersity $Đ$ and were shown to be biocompatible when evaluated using human fibroblast like cells. In addition, both polymers have been successfully used to fabricate dissolving MAPs that were either loaded with the antibiotic LEV or the antifungal agent ITRA. Drug deposition studies highlighted that the patches were able to administer up to ~ 1.9 mg of LEV (delivery efficiency: 94.7%) and ~ 0.2 mg of ITRA (delivery efficiency: 45.9%), respectively into *ex vivo* porcine skin. In addition, when the efficacy of the MAPs was investigated *in vitro* it was observed that all drug-loaded MAPs could inhibit the growth of *C. albicans* or *S. aureus*. However, more interestingly, we also found that even without any drug loading, blank MAPs fabricated from the acid form of polyAMPS could impose a level of inhibition on the growth of *C. albicans*. Although the current study highlights promising results in terms of the use of polyAMPS dissolving MAPs for the management of SSTI, further work focusing on translational aspects of the technology should be considered to bring such formulations from bench to bedside. For instance, additional work will be necessary to investigate if these MAPs are capable of breaching infected or inflamed skin tissues, or would these MAPs require an applicator to administer the formulation in a reproducible manner to the infection site. Nevertheless, the current study demonstrates that indeed the intradermal approach, *via* the use of polyAMPS based MAPs, is a promising drug delivery approach to manage SSTI.

CRediT authorship contribution statement

Akmal Hidayat Bin Sabri: Conceptualization, Methodology, Visualization, Investigation, Formal analysis, Data curation, Writing – original draft, Writing – review & editing. **Qonita Kurnia Anjani:** Conceptualization, Methodology, Visualization, Investigation, Validation, Formal analysis, Data curation, Writing – original draft, Writing – review & editing. **Pratik Gurnani:** Visualization, Investigation, Formal analysis, Writing – original draft. **Juan Domínguez-Robles:** Methodology, Formal analysis, Data curation, Investigation. **Natalia Moreno-Castellanos:** Methodology, Formal analysis, Data curation, Investigation. **Li Zhao:** Methodology, Investigation, Validation. **Aaron R.J. Hutton:** Methodology, Writing – review & editing. **Ryan F. Donnelly:** Resources, Writing – review & editing, Supervision, Funding acquisition.

Declaration of Competing Interest

The authors declare that they have no known competing financial interests or personal relationships that could have appeared to influence the work reported in this paper.

Data availability

Data will be made available on request.

Acknowledgement

The optical coherence tomography aspects of this work were funded by Wellcome Trust grant number WT094085MA

Appendix A. Supplementary material

Supplementary data to this article can be found online at https://doi.org/10.1016/j.ijpharm.2023.123292.

References

AMPS (2-Acrylamido-2-methylpropane sulfonic acid). Available at: https://atamankimya.com/sayfalar.asp?LanguageID=2&cid=3&id=11&id2=3631 [Accessed Sep 2022].

2-Acrylamido-2-methyl-1-propanesulfonic acid | C7H13NO4S - PubChem. Available at: https://pubchem.ncbi.nlm.nih.gov/compound/2-Acrylamido-2-methyl-1-propanesulfonic-acid#section=Melting-Point [Accessed Sep 2022].

2-Pyrrolidinone | C4H7NO - PubChem. Available at: https://pubchem.ncbi.nlm.nih.gov/compound/2-Pyrrolidinone. [Accessed Sep 2022].

Anjani, Q.K., et al., 2022. Soluplus®-based dissolving microarray patches loaded with colchicine: towards a minimally invasive treatment and management of gout. Biomater. Sci. https://doi.org/10.1039/d2bm01068b.

Anjani, Q., et al., 2023. Microarray patches for managing infections at a global scale. 359, 97–115.

Anjani, Q. K., Sabri, A. H. Bin, Utomo, E., Domínguez-Robles, J. & Donnelly, R. F. Elucidating the Impact of Surfactants on the Performance of Dissolving Microneedle Array Patches. *Mol. Pharm.* (2022). doi:10.1021/acs.molpharmaceut.1c00988.

Bhatnagar, S., Dave, K., Venuganti, V.V.K., 2017. Microneedles in the clinic. J. Control. Release 260, 164–182.

Boehm, R.D., et al., 2015. Polyglycolic acid microneedles modified with inkjet-deposited antifungal coatings. Biointerphases 10, 011004.

Boehm, R.D., et al., 2016. Inkjet deposition of itraconazole onto poly(glycolic acid) microneedle arrays. Biointerphases 11, 011008.

Botwina, P., et al., 2022. Self-organized nanoparticles of random and block copolymers of sodium 2-(acrylamido)-2-methyl-1-propanesulfonate and Sodium 11-(acrylamido) undecanoate as safe and effective zika virus inhibitors. Pharmaceutics 14, 1–16.

Colombo, M., Orthmann, S., Bellini, M., Staufenbiel, S., Bodmeier, R., 2017. Influence of drug brittleness, nanomilling time, and freeze-drying on the crystallinity of poorly water-soluble drugs and its implications for solubility enhancement. AAPS PharmSciTech. 18, 2437–2445.
Dong, X., et al., 2022. Keratinocyte-derived defensins activate neutrophil-specific receptors Mrgpra2a/b to prevent skin dysbiosis and bacterial infection. Immunity 55, 1645–1662.e7.
Donnelly, R.F., et al., 2009. Microneedle Arrays Allow Lower Microbial Penetration Than Hypodermic Needles In Vitro. 26, 2513–2522.
Douafer, H., Andrieu, V., Phanstiel, O., Brunel, J.M., 2019. Antibiotic adjuvants: make antibiotics great again! J. Med. Chem. 62, 8665–8681.
Edelsberg, J., et al., 2009. Trends in US hospital admissions for skin and soft tissue infections. Emerg. Infect. Dis. 15, 1516–1518.
Eliopoulos, G.M., Eliopoulos, C.T., 1988. Abtibiotic combinations: should they be tested? Clin. Microbiol. Rev. 1, 139–156.
Fairbanks, B.D., Gunatillake, P.A., Meagher, L., 2015. Biomedical applications of polymers derived by reversible addition - fragmentation chain-transfer (RAFT). Adv. Drug Deliv. Rev. 91, 141–152.
Farag, R.K., et al., 2020. Antibacterial and anti-fungal biological activities for acrylonitrile, acrylamide and 2-acrylamido-2-methylpropane sulphonic acid crosslinked terpolymers. Mater. (Basel). 13, 1–14.
Gill, H.S., Denson, D.D., Burris, B.A., Prausnitz, M.R., 2008. Effect of microneedle design on pain in human volunteers. Clin. J. Pain 24, 585–594.
Gimblet, C., et al., 2017. Cutaneous leishmaniasis induces a transmissible dysbiotic skin microbiota that promotes skin inflammation. Cell Host Microbe 22, 13–24.e4.
Gittard, S.D., et al., 2011. Deposition of antimicrobial coatings on microstereolithography-fabricated microneedles. J. Miner. Met. Mater. Soc. 63, 59–68.
Gittard, S.D., et al., 2013. The effects of geometry on skin penetration and failure of polymer microneedles. J. Adhes. Sci. Technol. 27, 227–243.
Gurnani, P., et al., 2020. PCR-RAFT: Rapid high throughput oxygen tolerant RAFT polymer synthesis in a biology laboratory. Polym. Chem. 11, 1230–1236.
Hespe, W., Meier, A. M. & Blankwater, Y. J. Excretion and distribution studies in rats with two forms of 14carbon-labelled polyvinylpyrrolidone with a relatively low mean molecular weight after intravenous administration - PubMed. *Arzneimittelforschung* 1158–1162 (1977). Available at: https://pubmed.ncbi.nlm.nih.gov/578432/. (Accessed: 25th July 2020).
Hua, C., et al., 2023. Necrotising soft-tissue infections. Lancet Infect. Dis. 23, e81–e94.
Joukhadar, C., et al., 2001. Impaired target site penetration of β-lactams may account for therapeutic failure in patients with septic shock. Crit. Care Med. 29, 385–391.
Kirkby, M., Sabri, A.B., Scurr, D.J., Moss, G.P., 2021. Dendrimer-mediated permeation enhancement of chlorhexidine digluconate: determination of in vitro skin permeability and visualisation of dermal distribution. Eur. J. Pharm. Biopharm. 159, 77–87.
Kirkby, M., Sabri, A.B., Scurr, D., Moss, G., 2022. Microneedle-mediated permeation enhancement of chlorhexidine digluconate. Pharm. Res. 39, 1945–1958.
Kurnia, Q., Hidayat, A., Sabri, B., Domínguez-robles, J., Donnelly, R.F., 2022. Metronidazole nanosuspension loaded dissolving microarray patches : an engineered composite pharmaceutical system for the treatment of skin and soft tissue infection. Biomater. Adv. 140.
Larrañeta, E., et al., 2014. A proposed model membrane and test method for microneedle insertion studies. Int. J. Pharm. 472, 65–73.
Lawrence, H. S. & Nopper, A. J. *Superficial Bacterial Skin Infections and Cellulitis. Principles and Practice of Pediatric Infectious Diseases: Fourth Edition* (Elsevier Inc., 2012). doi: 10.1016/B978-1-4377-2702-9.00070-2.
Martínez-Cornejo, V., et al., 2020. Synthesis of poly(2-acrylamido-2-methylpropane sulfonic acid) and its block copolymers with methyl methacrylate and 2-hydroxyethyl methacrylate by quasiliving radical polymerization catalyzed by a cyclometalated ruthenium(ii) complex. Polymers (Basel) 12.
McAlister, E., et al., 2020. Directly compressed tablets: a novel drug-containing reservoir combined with hydrogel-forming microneedle arrays for transdermal drug delivery. Adv. Healthc. Mater. 2001256.
McAlister, E., Kearney, M.C., Martin, E.L., Donnelly, R.F., 2021. From the laboratory to the end-user: a primary packaging study for microneedle patches containing amoxicillin sodium. Drug Deliv. Transl. Res. 1–17 https://doi.org/10.1007/s13346-020-00883-5.
Melander, R.J., Melander, C., 2017. The challenge of overcoming antibiotic resistance: an adjuvant approach? ACS Infect. Dis. 3, 559–563.
Mellaerts, R., et al., 2008. Increasing the oral bioavailability of the poorly water soluble drug itraconazole with ordered mesoporous silica. Eur. J. Pharm. Biopharm. 69, 223–230.
Moad, G. *Radical Polymerization. Polymer Science: A Comprehensive Reference, 10 Volume Set* **3**, (Elsevier B.V., 2012).
Nakatsuji, T., et al., 2013. The microbiome extends to subepidermal compartments of normal skin. Nat. Commun. 4, 1–8.
Nakatsuji, T., et al., 2013. The microbiome extends to subepidermal compartments of normal skin. Nat. Commun. 1–8 https://doi.org/10.1038/ncomms2441.
Palmer, G.H., Bankhead, T., Seifert, H.S., 2016. Antigenic variation in bacterial pathogens. Virulence Mech. Bact. Pathog. 4, 445–480.
Pasricha, R. & Sachdev, D. *Biological characterization of nanofiber composites. Nanofiber Composites for Biomedical Applications* (Elsevier Ltd, 2017). doi:10.1016/B978-0-08-100173-8.00007-7.
Peddinti, B.S.T., et al., 2019. Inherently self-sterilizing charged multiblock polymers that kill drug-resistant microbes in minutes. Mater. Horizons 6, 2056–2062.
Peltonen, L., Hirvonen, J., 2010. Pharmaceutical nanocrystals by nanomilling: critical process parameters, particle fracturing and stabilization methods. J. Pharm. Pharmacol. 62, 1569–1579.
Peng, K., et al., 2021. Dissolving microneedle patches loaded with amphotericin B microparticles for localised and sustained intradermal delivery : potential for enhanced treatment of cutaneous fungal infections. J. Control. Release 339, 361–380.
Peng, K., et al., 2021. Hydrogel-forming microneedles for rapid and efficient skin deposition of controlled release tip-implants. Mater. Sci. Eng. C 127.
Permana, A.D., et al., 2019. Solid lipid nanoparticle-based dissolving microneedles: a promising intradermal lymph targeting drug delivery system with potential for enhanced treatment of lymphatic filariasis. J. Control. Release 316, 34–52.
Permana, A.D., et al., 2020. Dissolving microneedle-mediated dermal delivery of itraconazole nanocrystals for improved treatment of cutaneous candidiasis. Eur. J. Pharm. Biopharm. 154, 50–61.
Rajan, S., 2012. Skin and soft-tissue infections: classifying and treating a spectrum. Cleve. Clin. J. Med. 79, 57–66.
Sabri, A., et al., 2019. Expanding the applications of microneedles in dermatology. Eur. J. Pharm. Biopharm. 140, 121–140.
Sabri, A. H. Bin, Anjani, Q. K., Utomo, E., Ripolin, A. & Donnelly, R. F. Development and characterization of a dry reservoir-hydrogel-forming microneedles composite for minimally invasive delivery of cefazolin. *Int. J. Pharm.* **617**, 121593 (2022).
Sachan, R., et al., 2017. Printing amphotericin B on microneedles using matrix- assisted pulsed laser evaporation. Int. J. Bioprinting 3, 147–157.
Semsarilar, M., Perrier, S., 2010. 'Green' reversible addition-fragmentation chain-transfer (RAFT) polymerization. Nat. Chem. 2, 811–820.
Tekko, I.A., et al., 2022. Novel bilayer microarray patch-assisted long-acting micro-depot cabotegravir intradermal delivery for HIV pre-exposure prophylaxis. Adv. Funct. Mater. 32, 2106999.
Veloz Martínez, I., Ek, J.I., Ahn, E.C., Sustaita, A.O., 2022. Molecularly imprinted polymers via reversible addition-fragmentation chain-transfer synthesis in sensing and environmental applications. RSC Adv. 12, 9186–9201.
Volpe-zanutto, F., et al., 2021. Artemether and lumefantrine dissolving microneedle patches with improved pharmacokinetic performance and antimalarial efficacy in mice infected with Plasmodium yoelii. 333, 298–315.
Volpe-Zanutto, F., et al., 2022. Hydrogel-forming microarray patches with cyclodextrin drug reservoirs for long-acting delivery of poorly soluble cabotegravir sodium for HIV Pre-Exposure Prophylaxis. J. Control. Release 348, 771–785.
Yamaoka, T., Tabata, T. & Ikada, Y. Comparison of Body Distribution of Poly (viny1 alcohol) with Other Water-soluble Polymers after Intravenous Administration. 479–486 (1995).
Zhang, C., et al., 2023. Development of dissolving microneedles for intradermal delivery of the long-acting antiretroviral drug bictegravir. Int. J. Pharm. 642, 123108.